

Mirages, anti-mirages, and further surprises in quantum corrals with non-magnetic impurities

Markus Schmid, Arno P. Kampf

Angaben zur Veröffentlichung / Publication details:

Schmid, Markus, and Arno P. Kampf. 2003. "Mirages, anti-mirages, and further surprises in quantum corrals with non-magnetic impurities." *Annalen der Physik* 12 (7-8): 463-70. <https://doi.org/10.1002/andp.200310023>.

Nutzungsbedingungen / Terms of use:

licgercopyright

Dieses Dokument wird unter folgenden Bedingungen zur Verfügung gestellt: / This document is made available under the following conditions:

Deutsches Urheberrecht

Weitere Informationen finden Sie unter: / For more information see:

<https://www.uni-augsburg.de/de/organisation/bibliothek/publizieren-zitieren-archivieren/publizieren>



Mirages, anti-mirages, and further surprises in quantum corrals with non-magnetic impurities

Markus Schmid* and Arno P. Kampf**

Theoretical Physics III, Center for Electronic Correlations and Magnetism, Institute of Physics, University of Augsburg, 86135 Augsburg, Germany

We investigate the local density of states (LDOS) for non-interacting electrons in a hard-wall ellipse in the presence of a single non-magnetic scattering center. Using a T-matrix analysis we calculate the local Green's function and observe a variety of quantum mirage effects for different impurity positions. Locating the impurity near positions with LDOS maxima for the impurity free corral can either lead to a reduction or an enhancement of the LDOS at the mirror image point, i.e. a mirage or anti-mirage effect, or even suppress LDOS maxima in the entire area of the corral.

1 Introduction

The technological advances in scanning tunneling microscopy (STM) have made it possible to manipulate individual atoms on metallic surfaces [1]. These remarkable achievements allow local measurements of electronic properties with a spatial resolution of atomic length scales even on artificially designed geometries for surface adatoms [2]. The experimental advances have led e.g. to the spectacular observation of mirage effects in elliptic quantum corrals of magnetic Co atoms on Cu (111) surfaces [3]. If an additional Co atom is placed at one of the foci of the ellipse, a Kondo resonance in the local density of states (LDOS) is not only observed at the magnetic ion itself but at the other, impurity free focus as well. The mirage effect can be viewed as a beautiful manifestation of quantum mechanical interference phenomena as a result of the multiple scattering events of the electrons from the atoms forming the boundary of the corral and from the impurity at one focus.

The theoretical work on this problem emphasised the many-body Kondo physics of itinerant electrons in the corral interacting with the localized magnetic moments of the impurities [4–7]. But it was also found that for the specific elliptic geometry even stronger mirage effects can be observed, if the additional impurity is moved slightly away from the focal point [6]. Furthermore, mirage effects may even be absent depending on the intrinsic level width [5] or for specific electron densities inside the elliptic corrals; one of the crucial quantities is the LDOS at the position where the additional adatom is placed. Therefore, already without invoking the Kondo physics the unique geometry of an elliptic corral appears to give rise to intriguing quantum mechanical effects which deserve a detailed analysis also for the significantly simpler problem of a non-magnetic impurity in a hard-wall corral.

* Corresponding author E-mail: markus.schmid@physik.uni-augsburg.de

** E-mail: arno.kampf@physik.uni-augsburg.de

Indeed we will show in this paper that a surprising variety of structures in the LDOS can be generated depending on the precise location of a single additional non-magnetic scattering center inside a hard-wall elliptic corral. At the mirror position of the local impurity potential the LDOS may be suppressed or even enhanced, and also the almost complete suppression of LDOS maxima can be achieved. These observations underline the richness of quantum mechanical interference phenomena in an elliptical geometry which may be verified experimentally.

2 Solution of the 2d Schrödinger equation in a hard-wall ellipse

In a first step we review the solution of the two-dimensional (2D) Schrödinger equation for non-interacting electrons in a hard wall ellipse. Following [8] it is convenient to introduce elliptical coordinates through the transformation [9]

$$\begin{aligned}x &= ae \cos(\theta) \cosh(\eta), \\y &= ae \sin(\theta) \sinh(\eta),\end{aligned}\tag{1}$$

where a denotes the semimajor axis and e is the eccentricity of the ellipse. In the new coordinates the Schrödinger equation takes the following form:

$$\left[-\frac{\hbar^2}{2m(ae)^2} \frac{2}{\cosh(2\eta) - \cos(2\theta)} \left(\frac{\partial^2}{\partial\theta^2} + \frac{\partial^2}{\partial\eta^2} \right) + V(\eta) \right] \psi(\theta, \eta) = \epsilon\psi(\theta, \eta)\tag{2}$$

where m is the electron mass and ϵ is the energy eigenvalue. Due to the hard-wall condition the potential V vanishes inside the elliptic corral and is infinite otherwise. Using the factorized ansatz for the eigenfunctions

$$\psi(\theta, \eta) = \Theta(\theta)\Phi(\eta)\tag{3}$$

the Schrödinger equation inside the ellipse ($V(\eta) = 0$) is rearranged as

$$-\left[\frac{\partial^2}{\partial\theta^2} - 2k \cos(2\theta) \right] \Theta(\theta) = \left[\frac{\partial^2}{\partial\eta^2} + 2k \cosh(2\eta) \right] \Phi(\eta)\tag{4}$$

where $k = (ae)^2 m\epsilon / 2\hbar^2$. The Schrödinger equation thus separates with respect to the elliptic coordinates θ and η and reduces to the two differential equations

$$\frac{\partial^2}{\partial\theta^2} \Theta(\theta) + (\alpha - 2k \cos(2\theta)) \Theta(\theta) = 0,\tag{5}$$

$$\frac{\partial^2}{\partial\eta^2} \Phi(\eta) - (\alpha - 2k \cosh(2\eta)) \Phi(\eta) = 0\tag{6}$$

where α is a separation constant. Eqs. (5) and (6) are the Mathieu equation and the modified Mathieu equation, respectively [9, 10].

Since θ is the polar angle and thus $\Theta(\theta + 2\pi) = \Theta(\theta)$ we select the periodic solutions of Eq. (5), which are the Mathieu functions of the first kind of integral order [9]. We obtain two types of solutions:

$$\Theta_r(\theta) = ce_r(\theta, k^c) \quad \text{or}\tag{7}$$

$$\Theta_r(\theta) = se_r(\theta, k^s)\tag{8}$$

where “ce” and “se” are the abbreviations for “cosine-elliptic” and “sine-elliptic” introduced by Whittaker [9]. Due to the periodicity condition there exists only a discrete set of numbers $\alpha = \alpha_r(k)$ for fixed k [10]. The index r in Eqs. (7) and (8) denotes the order of the Mathieu functions of the first kind.

The solutions of Eq. (6), which are necessarily restricted to the same set of numbers $\alpha_r(k)$ as the corresponding solution of (5), are

$$\Phi_r(\eta) = \text{Ce}_r(\eta, k^c), \quad \text{or} \quad (9)$$

$$\Phi_r(\eta) = \text{Se}_r(\eta, k^s). \quad (10)$$

Ce and Se in Eqs. (9) and (10) denote the modified Mathieu functions of the first kind of integral order [9]. They must meet the hard-wall condition $\Phi_r(\eta_0) = 0$ at the boundary line of the ellipse, which leads to a discrete set of values k_n . This implies that the discrete sets for k_n^c and k_n^s must meet the conditions

$$\Phi_r(\eta_0) = \text{Ce}_r(\eta_0, k_n^c), \quad \text{or} \quad (11)$$

$$\Phi_r(\eta_0) = \text{Se}_r(\eta_0, k_n^s). \quad (12)$$

Therefore, k_n^c and k_n^s are the n^{th} zeroes of $\text{Ce}_r(\eta_0, k^c)$ and $\text{Se}_r(\eta_0, k^s)$, respectively, for fixed r . η_0 is directly related to the eccentricity e of the ellipse through

$$e = \frac{1}{\cosh(\eta_0)}. \quad (13)$$

Altogether we find the following form of the exact eigenstates inside the hard-wall ellipse [8]:

$$\psi_{r,n_c}^c(\theta, \eta) = c e_r(\theta, k_n^c) \text{Ce}_r(\eta, k_n^c), \quad (14)$$

$$\psi_{r,n_s}^s(\theta, \eta) = s e_r(\theta, k_n^s) \text{Se}_r(\eta, k_n^s). \quad (15)$$

r , n and $c(s)$ enumerate the quantum numbers for the eigenstates; the eigenenergies are determined by the hard-wall condition and the periodicity requirement for the Mathieu functions. Note that $c e_r$, $s e_r$ and Ce_r , Se_r are all real. The symmetry under reflection at the semimajor axis is even for the $c e_r$ function (cosine-elliptic) and odd for the $s e_r$ function (sine-elliptic) for each r . Moreover the parity of $c e_r$ and $s e_r$ is even/odd, if r is even/odd. Specifically,

$$\psi_r^c(-\theta, \eta) = \psi_r^c(\theta, \eta), \quad (16)$$

$$\psi_r^s(-\theta, \eta) = -\psi_r^s(\theta, \eta), \quad (17)$$

$$\psi_{2r}^{c/s}(\theta + \pi, \eta) = \psi_{2r}^{c/s}(\theta, \eta), \quad (18)$$

$$\psi_{2r+1}^{c/s}(\theta + \pi, \eta) = -\psi_{2r+1}^{c/s}(\theta, \eta). \quad (19)$$

In the following we will specifically investigate an ellipse with eccentricity $e = 0.5$. The energy scale for the eigenenergies is furthermore determined by the size of the ellipse, i.e. the length of the semimajor axis a . For a specific choice for a we orient ourselves at the typical size of the elliptic corral of Co atoms on a Cu (111) surface used in the experiments of Manoharan et al. in [3] for which $a \sim 71$ Å. In this setup the Fermi energy ϵ_F is 450 meV which corresponds to the energy of the 42nd eigenstate, and due to the spin degeneracy amounts to a particle number of 84 electrons inside the ellipse. For the specific choice for the size of the ellipse the ground state energy

$$E_0 = k_0 \frac{2\hbar^2}{(ae)^2 m} \quad (20)$$

is $E_0 = 13$ meV. For fixed eccentricity $e = 0.5$ and $k_n = k_{42}$ the wavefunction of the eigenstate at the Fermi energy has a high probability density at the two foci of the ellipse – a precondition to observe strong mirage effects when an additional impurity atom is placed at one of the focal points.

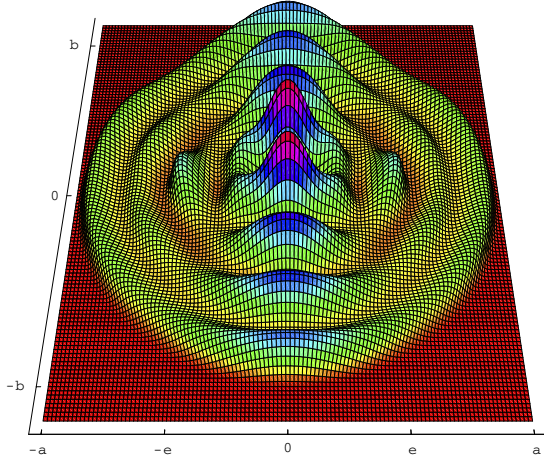


Fig. 1 LDOS $N_0(\mathbf{r}, \epsilon_{42})$, $\epsilon_{42} = \epsilon_F$, for non-interacting electrons inside an ellipse with semimajor axis a (horizontal) and semiminor axis b (vertical). This viewpoint is the same for all plots in Figs. 1–4. The scale of the LDOS can be taken from Figs. 5–7.

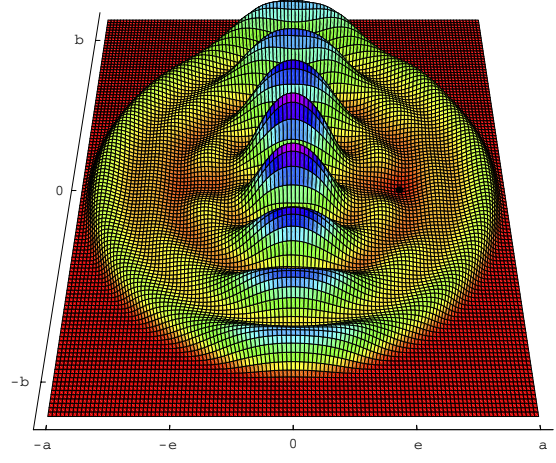


Fig. 2 LDOS $N(\mathbf{r}, \epsilon_{42})$ with an impurity (\bullet) at the right focus $\mathbf{r}_0 = (ea, 0)$; $U = 16.6E_0A$ ($A = \pi ab$ is the area of the ellipse).

3 The scattering problem

The LDOS of the non-interacting electron system inside the corral is easily obtained from the retarded one-particle Green's function

$$G_0^{ret}(\mathbf{r}, \mathbf{r}', \epsilon) = \sum_j \frac{\psi_j(\mathbf{r})\psi_j^*(\mathbf{r}')}{\epsilon - \epsilon_j + i\delta} \quad (21)$$

where the eigenfunctions ψ_j are given by Eqs. (14) and (15) and ϵ_j is the corresponding eigenenergy of the j^{th} eigenstate. The free LDOS $N_0(\mathbf{r}, \epsilon)$ then follows from

$$N_0(\mathbf{r}, \epsilon) = -\frac{1}{\pi} \text{Im} G_0(\mathbf{r}, \mathbf{r}, \epsilon). \quad (22)$$

In Fig. 1 we present the LDOS at the Fermi energy $\epsilon_F = \epsilon_{42}$ using a finite broadening $\delta = \langle \Delta\epsilon \rangle = 0.77E_0$ where $\langle \Delta\epsilon \rangle$ is the average level spacing of the eigenenergy spectrum ($\delta = 10$ meV for the parameters mentioned above for the ellipse with $a = 71$ Å). While the eigenstates of the hard-wall ellipse are naturally sharp ($\delta = 0$), in actual experiments the lifetime of the surface electrons is finite e.g. because of the imperfect hard-wall condition. Using a finite broadening is therefore reasonable not only for practical purposes. We note that $N_0(\mathbf{r}, \epsilon_{42})$ is dominated by the contributions of the 42nd and 43rd state, because the energy difference between these states is seven times smaller than the energy difference between 41st and 42nd state.

Next we add a non-magnetic impurity scattering center to the ellipse at point \mathbf{r}_0 , which we model by a local delta-function potential

$$V(\mathbf{r}) = U\delta(\mathbf{r} - \mathbf{r}_0). \quad (23)$$

The electronic scattering processes are thus described by the scattering T-matrix

$$T(\mathbf{r}_0, \epsilon) = \frac{U}{1 - UG_0^{ret}(\mathbf{r}_0, \mathbf{r}_0, \epsilon)}. \quad (24)$$

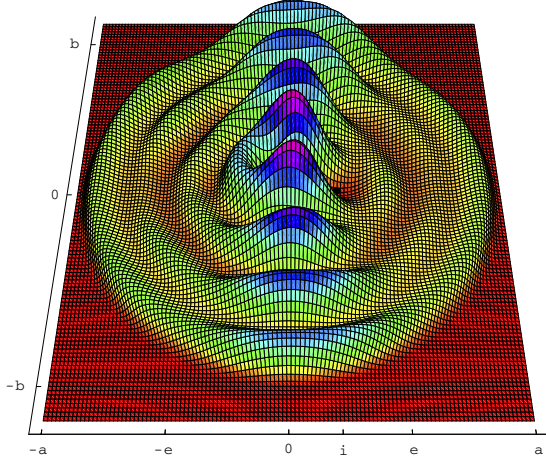


Fig. 3 LDOS $N(\mathbf{r}, \epsilon_{42})$ with an impurity (\bullet) at $\mathbf{r}_0 = (i, 0) = (0.22a, 0)$; $U = 16.6E_0A$.

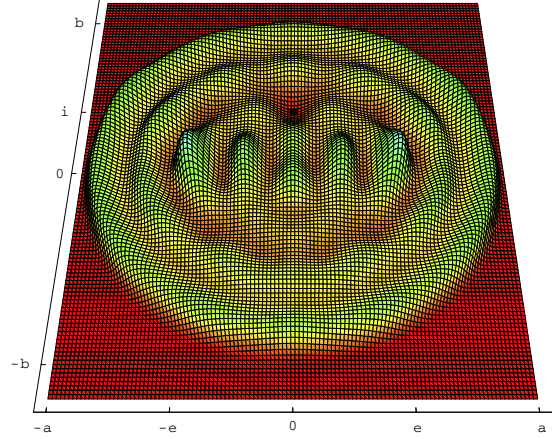


Fig. 4 LDOS $N(\mathbf{r}, \epsilon_{42})$ with an impurity (\bullet) at $\mathbf{r}_0 = (i, 0) = (0, 0.33a)$; $U = 16.6E_0A$.

The electronic propagator in the presence of the impurity potential follows then as

$$G(\mathbf{r}, \mathbf{r}', \epsilon) = G_0^{ret}(\mathbf{r}, \mathbf{r}', \epsilon) + G_0^{ret}(\mathbf{r}, \mathbf{r}_0, \epsilon)T(\mathbf{r}_0, \epsilon)G_0^{ret}(\mathbf{r}_0, \mathbf{r}', \epsilon), \quad (25)$$

and the modified LDOS is

$$N(\mathbf{r}, \epsilon) = -\frac{1}{\pi} \text{Im} G(\mathbf{r}, \mathbf{r}, \epsilon). \quad (26)$$

In our subsequent analysis we will choose selected points for the position of the impurity and explore the consequences for the LDOS in the entire area of the elliptical corral.

4 Results

As mentioned above, Fig. 1 shows the free LDOS at the energy $\epsilon = \epsilon_{42}$ and for $\delta = 0.77E_0$. The contribution of the 43rd state is very strong along the semiminor axis and leads to a sequence of local maxima and minima. On the other hand the contributions of the 42nd state are responsible for the structure of the LDOS in the other parts of the corral especially near the foci.

Fig. 2 shows the LDOS when the impurity is placed at the right focus; the position of the impurity is indicated in the figure by a black bullet. With increasing potential strength U one observes that the LDOS is reduced essentially everywhere except for the positions of the minima of the free LDOS and the maxima along the semiminor axis, where it remains almost constant. The evolution of the LDOS with increasing U is shown in Fig. 5 for a cut along the semimajor axis. At the impurity-free focus the LDOS continuously decreases with increasing U . Importantly, the LDOS is almost symmetrically suppressed at the other impurity-free focus; this phenomenon can be ascribed to the previously studied so-called quantum mirage effect. Here we use this acronym to underline that the LDOS at both focal points is changing in the same manner. We emphasize again that the ridge structure with its high maxima along the semiminor axis is conserved. So, although the impurity is only at the right focus, the semiminor and the semimajor axis still appear like symmetry axes – at least within the resolution of the chosen color grid. This is the quantum mirage. A similar mirage effect persists also, when the impurity is moved slightly away from the focus [5].

A very different behavior of the LDOS is observed, if the impurity is placed at the position of the first maximum of the free LDOS on the semimajor axis near the center of the ellipse. This is shown in Fig. 3,

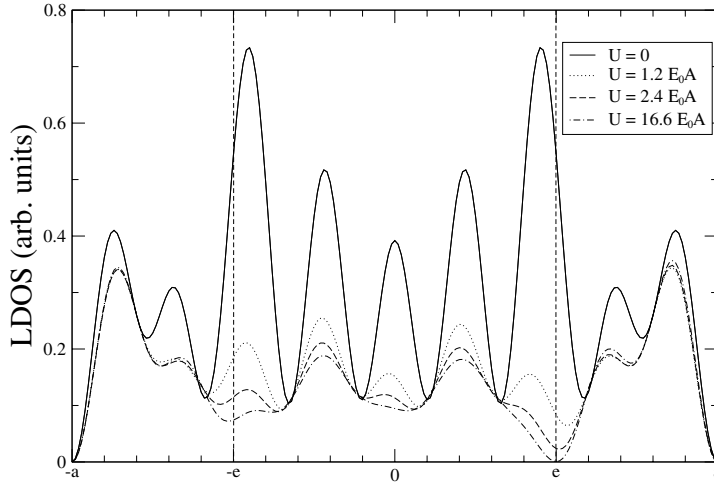


Fig. 5 LDOS $N(\mathbf{r}, \epsilon)$ for a cut along the semimajor axis; the impurity is at the right focus. The vertical dashed lines serve as a guide to the eye to compare the LDOS at the impurity with the LDOS at the mirror position.

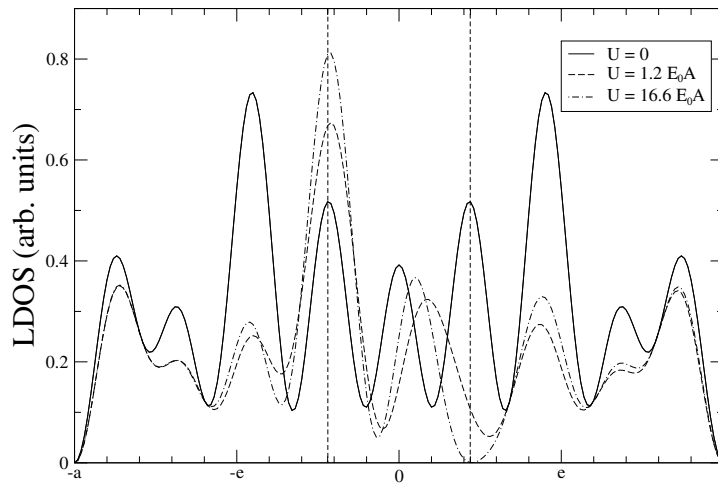


Fig. 6 LDOS $N(\mathbf{r}, \epsilon_{42})$ for a cut along the semimajor axis with the impurity at the position $\mathbf{r}_0 = (0.22a, 0)$.

and the corresponding cut along the semimajor axis is shown in Fig. 6. Again, as expected, the LDOS in the presence of the impurity is reduced with increasing U almost everywhere inside the corral. But, surprisingly, the opposite effect is observed at the mirror image point of the impurity position with respect to a reflection at the origin. There the impurity causes in fact an enhancement of the LDOS. Thus, in this case the interference pattern for the perturbed electronic wavefunctions leads just to the opposite effect as in the above discussed quantum mirage in Fig. 2; we therefore call this observation an anti-mirage effect. Note that in the rest of the corral the shape of the impurity LDOS remains very symmetric, but with a slight overall enhancement of the LDOS in the left part of the ellipse. Similar as in Fig. 2 the maxima of the ridge structure along the semiminor axis persist almost unchanged. One can observe the anti-mirage effect also when the impurity is put somewhere between $\mathbf{r}_0 = (0.16a, 0)$ and the second minimum at $\mathbf{r}_0 = (0.33a, 0)$.

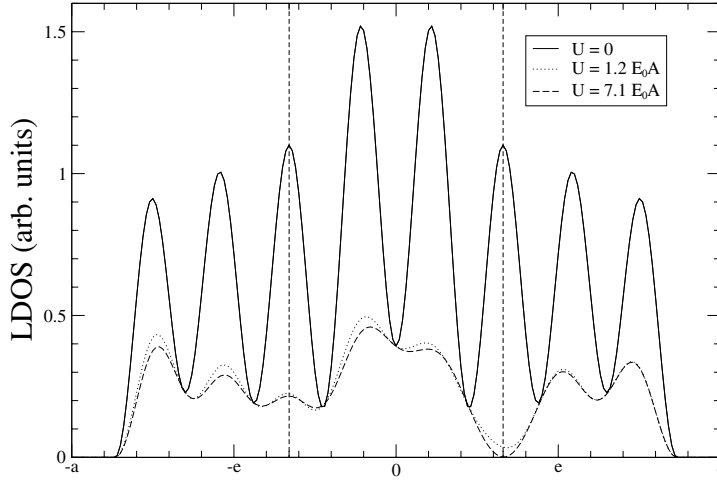


Fig. 7 LDOS $N(\mathbf{r}, \epsilon_{42})$ for a cut along the semiminor axis with the impurity at $\mathbf{r}_0 = (0, 0.33a)$.

In a third example we place the impurity at the second maximum along the semiminor axis away from the center (see Fig. 4 and Fig. 7). This particular impurity position has the remarkable consequence that the ridge structure along the semiminor axis is entirely wiped out, and what is left is very similar to the probability density of the 42nd state. This phenomenon occurs for every impurity position at any of the local maxima along the semiminor axis. For example, if the impurity is placed at the points with the highest LDOSs of the elliptic corral, the LDOS reacts most sensitively. This in itself may not appear as a surprise, because a local perturbation at the space point with the highest probability density should indeed lead to severe changes in the local electronic structure. Yet, the total wipeout of the ridges comes as a spectacular surprise. If the impurity is placed at a minimum along the semiminor axis, the resulting LDOS appears essentially unaffected.

We note that the LDOS strongly depends on the electronic density in the corral, i.e. the spatial structure of the eigenstates at or close to the Fermi energy. Different situations can be realized by varying the length of the semimajor axis at fixed electronic density. They can be physically achieved by studying different corral sizes on identical substrates. For example, the energies of the 42nd and the 43rd state are very close to each other so that the LDOSs with the same broadening δ at the eigenenergies ϵ_{42} and ϵ_{43} are nearly the same. On the other hand, the LDOSs at energies ϵ_{41} and ϵ_{44} have a significantly different structure. In particular, the LDOSs $N(\mathbf{r}, \epsilon_{41})$ and $N(\mathbf{r}, \epsilon_{44})$ nearly vanish at the foci. The quantum mirage effects as arising from placing impurities near the foci, are in this case essentially unobservable. In this sense, the size of the corrals of Co atoms as realized in the experiments was a lucky choice for detecting the mirage phenomena.

5 Summary

We have identified three distinctly different interference phenomena for non-magnetic impurity induced changes in the LDOS of non-interacting electrons in elliptic hard-wall quantum corrals. Mirage or anti-mirage effects occur depending on the impurity position inside the corral. Even an almost complete suppression of pronounced rich structures in the LDOS can be achieved for special choices of the impurity location. These surprising phenomena are a manifestation of quantum mechanical interference effects which may be tested experimentally with the already existing elliptic quantum corrals on metallic surfaces.

Acknowledgements We thank M. Sekania, R. Bulla, N. Tong, and X. Ren for assistance and helpful discussions. This work was supported by the Deutsche Forschungsgemeinschaft through SFB 484.

References

- [1] D. M. Eigler and E. K. Schweitzer, *Nature* **344**, 524 (1990).
- [2] For a recent review see G. A. Fiete and E. J. Heller, *Rev. Mod. Phys.* **75**, 933 (2003).
- [3] H. C. Manoharan, C. P. Lutz, and D. M. Eigler, *Nature* **403**, 512 (2000).
- [4] O. Agam and A. Schiller, *Phys. Rev. Lett.* **86**, 484 (2001).
- [5] A. Lobos and A. A. Aligia, *Phys. Rev. B* **68**, 035411 (2003).
- [6] A. A. Aligia, *Phys. Rev. B* **64**, 121102 (2001).
- [7] G. Chiappe and A. A. Aligia, *Phys. Rev. B* **66**, 075421 (2002).
- [8] D. Porras, J. Fernández-Rossier, and C. Tejedor, *Phys. Rev. B* **63**, 155406 (2001).
- [9] N. W. McLachlan, *Theory and Applications of Mathieu Functions* (Dover Publications, New York, 1964).
- [10] M. Abramowitz and I. A. Stegun, *Handbook of Mathematical Functions* (Dover Publications, New York, 1965).